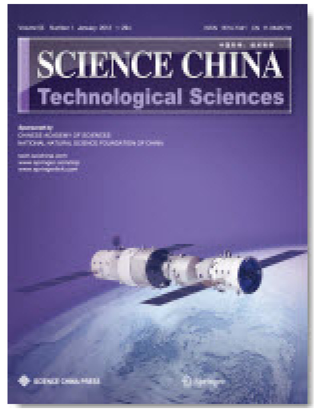

Defect-mode and Fabry-Perot resonance induced multi-band nonreciprocal thermal radiation

Journal:	*Science China Technological Sciences*
Manuscript ID	SCTS-2023-0435.R3
Manuscript Type:	Original Article
Date Submitted by the Author:	17-Nov-2023
Complete List of Authors:	Chen, Zihe; Huazhong University of Science and Technology Yu, Shilv; Huazhong University of Science and Technology Yuan, Cheng; Wuhan Fiberhome Fuhua Electric Co., Ltd Cui, Xinyou; Wuhan Fiberhome Fuhua Electric Co., Ltd Hu, Run; Huazhong University of Science and Technology,
Keywords:	Kirchhoff’s law, multi-band nonreciprocal thermal radiation, magnetophotonic crystal, Tamm plasmon, defect layer, Fabry-Perot resonance
Speciality:	Engineering Thermophysics, Optics

Defect-mode and Fabry-Perot resonance induced multi-band nonreciprocal thermal radiation

Zihe Chen[1], Shilv Yu[1], Cheng Yuan[2], Xinyou Cui[2], Run Hu[1]*

[1]School of Energy and Power Engineering, Huazhong University of Science and Technology, Wuhan 430074, China

[2]Wuhan Fiberhome Fuhua Electric Co., Ltd, Wuhan 430074, China

*Email: hurun@hust.edu.cn

Abstract: According to Kirchhoff's radiation law, the spectral-directional absorptivity (α) and spectral-directional emissivity (e) of an object are widely believed to be identical, which places a fundamental limit on photonic energy conversion and management. The introduction of Weyl semimetals and magneto-optical (MO) materials into photonic crystals makes it possible to violate Kirchhoff's law, but most existing work only report the unequal absorptivity and emissivity spectra in single band, which cannot meet the requirements of most practical applications. Here, we introduce defect layer into the structure composed by one-dimensional (1D) magnetophotonic crystal and a metal layer, which realizes dual-band nonreciprocal thermal radiation under a 3T magnetic field with an incident angle of 60°. The realization of dual-band nonreciprocal radiation is mainly due to the Fabry-Perot (FP) resonance occurring in the defect layer and the excitation of Tamm plasmon, which is proved by calculating the magnetic field distribution. In addition, the effects of incident angle and structural parameters on nonreciprocity are also studied. What's more, the number of nonreciprocal bands could be further increased by tuning the defect layer thickness. When the defect layer thickness increases to 18.2 μm, tri-band nonreciprocal thermal radiation is realized due to the enhanced number of defect modes in the photonic band gap and the FP resonance occurring in the defect layer. Finally, the effect of defect location on nonreciprocity is also discussed. The present work provides a new way for the design of multi-band or even broad-band nonreciprocal thermal emitters.

Keywords: Kirchhoff's law, multi-band nonreciprocal thermal radiation, magnetophotonic crystal, Tamm plasmon, defect layer, Fabry-Perot resonance

1. Introduction

Thermal radiation, one of the three forms of heat transfer, is widely used in energy harvest, transmission, conversion and other fields [1-4]. In the last few decades, the design of high-efficiency thermal emitters has been provided with the development of nanophotonic technology, which is aimed at the efficient utilization of thermal radiation [5, 6]. However, most current thermal emitters require that the emissivity e for a given angle and frequency is same to the absorptivity α, i.e. $e(\theta,\lambda)=\alpha(\theta,\lambda)$ [7, 8], which is the limitation of Kirchhoff's law.

Under this law, when an object absorbs thermal radiation from the heat source, it must also emit energy to the heat source in the same direction, which will result in an inherent loss of energy [9-12]. Therefore, violating this detailed balance for higher energy recovery is necessary and meaningful.

Theoretically, Kirchhoff's law is not the requirement of the law of thermodynamics, but the result of the Lorentz reciprocity theorem [13]. In other words, the thermal emitters composed of nonreciprocal materials can break the restriction of Kirchhoff's law under certain conditions [14, 15], so as to realize the separate control of absorption and emission processes. For example, the utilization of MO materials can make the time-reversal symmetry break with an external excitation, so they are one of the ideal candidates for realizing nonreciprocal thermal radiation [16]. Despite promising prospects, the perfect nonreciprocal thermal emitters, i.e., $|\alpha - e| \rightarrow 1$, are still difficult to achieve. In 2014, Fan's group [14] firstly designed a photonic crystal structure composed by an *n*-InAs grating structure and a metal layer. When the magnetic field *B* is 3 T, such structure demonstrates that the values of e and α are no longer equal, and the difference of $|\alpha - e|$ is close to 1 when the wavelength is 16 μm. Later on, in 2019, in order to reduce application condition, Zhao et al. [17] proposed a nanophotonic design consisting of a SiC grating and a MO material InAs at the bottom. However, the grating structure is difficult to be processed and not easy to be prepared on a large scale, which makes it difficult to be applied in practice [18-20]. To simplify the fabrication process, Wu et al. [21] proposed a 1D film structure composed of MO layer and spacer layer, which achieved the violation of Kirchhoff's law with a large magnetic field when the angle of incidence is 30°. More recently, type-I Weyl semimetals were found to be able to realize nonreciprocal radiation without an external excitation [15, 22-24]. For example, Chen et al. [24] proposed an optical nanostructure where a low-loss dielectric grating was added onto a semi-infinite magnetic Weyl semimetal, which can break Kirchhoff's law without any external stimulus. Nevertheless, all of these studies can only achieve single-band nonreciprocal thermal radiation, but most practical applications may require dual-band and even multi-band such as mid-infrared stealth, detectors, filters and so on [25, 26]. Therefore, it is necessary to pay more attention on the design of dual-band and multi-band nonreciprocal thermal emitters.

Currently, the structures of nonreciprocal emitters mainly include 1D photonic crystal structure and grating structure. However, the grating structure is more complicated to fabricate due to the need of lithography technology. Therefore, more attention has been paid to the realization of multilayer nonreciprocal thermal emitters. The existing designs of dual-band and even multi-band nonreciprocal thermal emitters mainly include topological photonic crystal structures [27], epsilon-near-zero (ENZ) multilayer structures [28], and Thue-Morse multilayer structures [29]. More recently, we also proposed a design method for multi-band nonreciprocal multilayer thermal emitters [30]. However, due to the limitation of machining accuracy, the existence of defects in photonic crystals is a non-negligible problem in actual processing. The effect of defects on the properties of photonic crystals in reciprocal systems has been studied extensively [31-34], but the effect of defect layers on the nonreciprocal thermal radiation is rarely studied. More recently, the integrated design of the Weyl semimetal and a photonic crystal with a defect layer can achieve the enhancement of the quality factor of nonreciprocal thermal radiation [22]. However, the influence of the defect layer on dual-band and even multi-band nonreciprocity is rarely reported.

In this work, we introduce the defect layer in 1D magnetophotonic crystals to achieve the dual-band nonreciprocal thermal radiation. On this basis, we find that with the increase of defect layer thickness, tri-band nonreciprocal emitter can be designed theoretically. The mechanism behind it is the excitation of Tamm plasmons and the FP resonance occurring in the defect layer, which can be proved by calculating the magnetic field distribution. Finally, the influences of incident angle, geometrical dimensions and defect layer location on the nonreciprocal radiation are also investigated.

2. Theoretical model and method

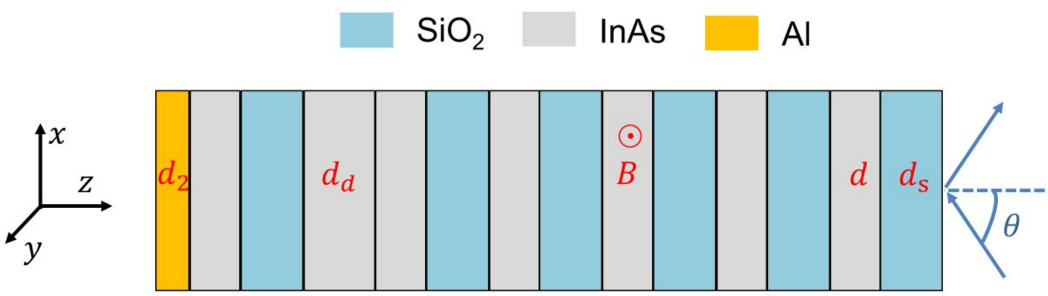

Figure 1. Schematic of magnetophotonic crystal multilayer structure containing the defect layer.

The nonreciprocal emitter we proposed is shown in Figure 1, which is composed by a magnetophotonic crystal with a defect layer and the bottom metal layer Al. In this work, the magnetophotonic crystal is a 12-layer structure which consists of the MO material *n*-InAs and dielectric material SiO_2 and the unit layer thickness of the two materials is d and d_s, respectively. The defect layer is assumed as the MO material *n*-InAs and its thickness is d_d. In addition, a magnetic field B is along the y axis. Under the influence of external magnetic field, the relative permittivity tensor of the doped InAs is nonsymmetric, and the specific expression is [35]

$$\varepsilon = \begin{bmatrix} \varepsilon_{xx} & 0 & \varepsilon_{xz} \\ 0 & \varepsilon_{yy} & 0 \\ \varepsilon_{zx} & 0 & \varepsilon_{zz} \end{bmatrix} \tag{1}$$

where

$$\varepsilon_{xx} = \varepsilon_{zz} = \varepsilon_{\infty} - \frac{\omega_p^2(\omega + i\Gamma)}{\omega\left[(\omega + i\Gamma)^2 - \omega_c^2\right]}, \tag{2}$$

$$\varepsilon_{xz} = -\varepsilon_{zx} = i\frac{\omega_p^2\omega_c}{\omega\left[(\omega + i\Gamma)^2 - \omega_c^2\right]}, \tag{3}$$

$$\varepsilon_{yy} = \varepsilon_{\infty} - \frac{\omega_p^2}{\omega(\omega + i\Gamma)}, \tag{4}$$

The specific definitions and values of the above parameters are from the Ref.[17]. The refractive index of the silicon dioxide is set at 1.45 and the permittivity of the metal Al is calculated by using the Drude model [17]

$$\varepsilon_{Al} = \varepsilon_{\infty} - \frac{\omega_p^2}{\omega(\omega + i\Gamma)} \quad , \tag{5}$$

Here, $\varepsilon_{\infty} = 1$, $\omega_p = 2.24\times10^{16}$ rad/s and $\Gamma = 1.24\times10^{14}$ rad/s [17].

In addition, only TM polarization wave in the *x-z* plane is considered and the angle of incidence is θ. The emissivity (e) and absorptivity (α) of this structure can be obtained by the calculations of the reflectivity and transmittance. Here, due to the high reflectivity of the metal Al, transmission processes are not considered. Therefore, the specific formulas of the α and e are [14]

$$\alpha(\theta,\lambda) = 1 - R(\theta,\lambda), \tag{6}$$

$$e(\theta,\lambda) = 1 - R(-\theta,\lambda), \tag{7}$$

The parameters $R(\theta,\lambda)$ and $R(-\theta,\lambda)$ are reflections of the angles of incidence θ and $-\theta$, respectively. The values of the corresponding reflection are calculated by using the transfer matrix method (TMM) and specific details can refer to Ref. [16, 35].

3. Results and discussion

In this work, the *B* is first set to 3T, and it can be achievable in practice. On this basis, in order to obtain high emissivity, the material thickness is optimized, and the optimal results are as follows: d = 1.7μm, d_s = 3.1μm, d_d = 7.4μm and d_2 (the thickness of the metal Al) = 0.2μm. The angle of incidence θ is 60°. Here, in order to facilitate the distinction between different structures, $(AC)^6M$ represents the structure without a defect layer and $(AC)^5D(AC)M$ represents the structure containing a defect layer, in which the letters A, C, D and M respectively represent SiO_2, InAs, defect layer and metal layer.

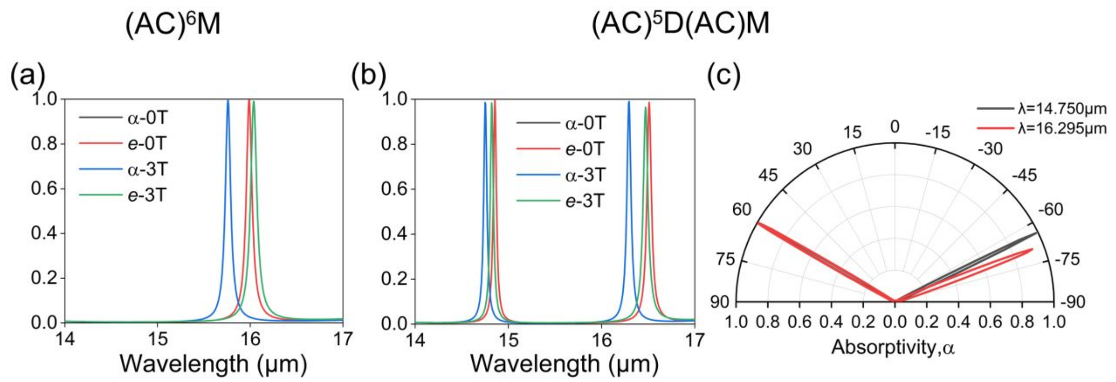

Figure 2. Absorptivity (α) and emissivity (e) spectra at θ=60° with B = 0T and B = 3T: (a) the structure without the defect layer ($(AC)^6M$), (b) the structure with the defect layer ($(AC)^5D(AC)M$). (c) Angular distribution diagram of absorptivity at the resonant wavelengths with B = 3T for the structure $(AC)^5D(AC)M$.

Figure 2(a) shows the emissivity and absorptivity spectra of the structure $(AC)^6M$. It can be seen that the emissivity and absorptivity spectra are overlapped without an external excitation, i.e., $e(\theta,\lambda)=\alpha(\theta,\lambda)$. In this case, the structure is reciprocal and follows Kirchhoff's law. In addition, the sharp emission or absorption peak is achieved, which is mainly because that Tamm plasmons is excited between the interface of the metal and photonic crystal. In contrast, when the applied magnetic field increases to 3T, the emissivity and absorptivity spectra no longer coincide, i.e., $e(\theta,\lambda)\neq\alpha(\theta,\lambda)$. At the wavelengths of 15.760μm and 16.035μm, the difference between absorptivity and emissivity can approach 1, which shows the strong nonreciprocity. After introducing the defect into the structure, the emissivity and absorptivity spectra are calculated as shown in Figure 2(b). Similarly, when B = 0T, there is no nonreciprocity. The difference is that another absorption (emission) peak occurs at the wavelength of 14.855μm and the original peak is redshifted. With B = 3T, both emission and absorption peaks show blueshift. The emissivity and absorptivity spectra also do not overlap with each other. The values of $|\alpha-e|$ at the wavelengths of 14.750μm and 16.295μm can reach 0.912 and 0.957, respectively, which exhibits the dual-band strong nonreciprocal thermal radiation and demonstrates that the existence of defect layer can lead to the occurrence of dual-band nonreciprocal radiation. Then, the angular distributions of the absorptivity with B = 3T at the wavelengths of 14.750μm and 16.295μm are calculated and the results are shown in Figure 2(c). It is obvious that the absorptivity is asymmetrical in spatial distribution, which is mainly attributed to the effect of MO effect caused by InAs with an external excitation.

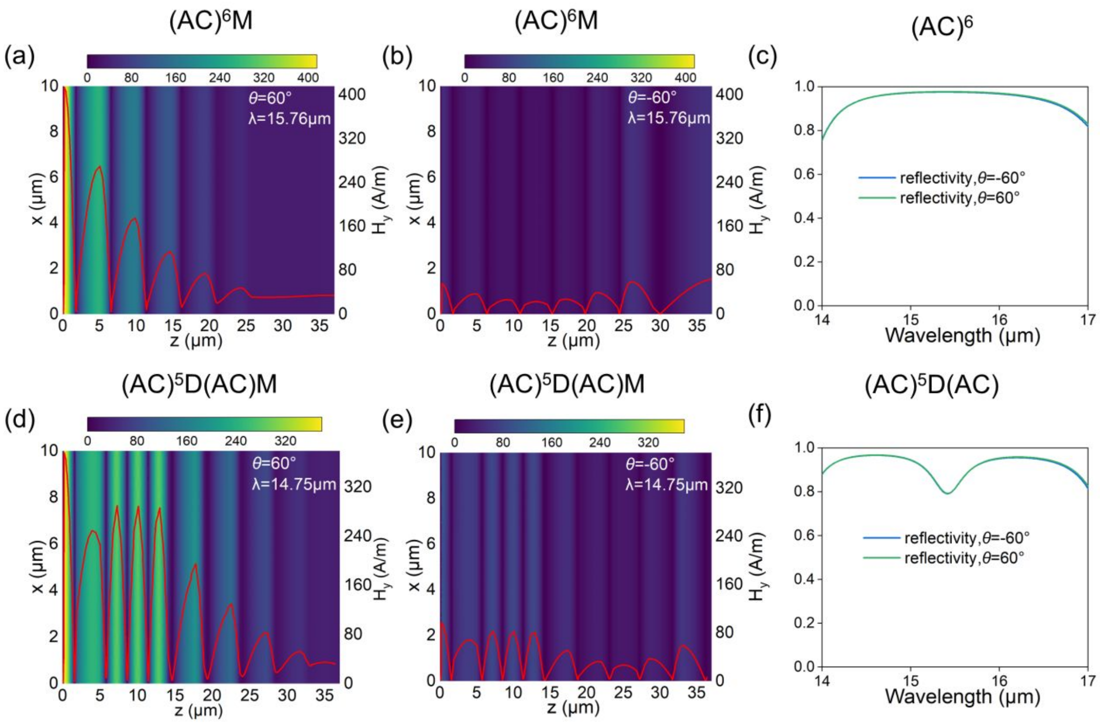

Figure 3. Magnetic field distribution ($|H_y|$) of the structure (AC)^{6}M along the z direction at the wavelength of 15.760μm (a) at $\theta = 60°$ and (b) $\theta = -60°$ with $B = 3$T. (c) The reflectivity spectra for the structure (AC)^6 at $\theta=60°$ and -60°. Magnetic field distribution ($|H_y|$) of the structure (AC)^{5}D(AC)M along the z direction at the wavelength of 14.750μm (d) at $\theta = 60°$ and (e) $\theta = -60°$ with $B = 3$T. (f) The reflectivity spectra for the structure (AC)^{5}D(AC) at $\theta = 60°$ and -60°.

In order to better explain the mechanism behind it, the magnetic field distribution at the resonant wavelength is calculated. When there is no defect in the photonic crystal, the magnetic field distributions along the z direction at the wavelength of 15.760μm with $\theta = 60°$ and $\theta = -60°$ are shown in Figure 3(a) and (b). It is obvious that the magnetic field amplitude is greatly enhanced at the junction of metal and magnetophotonic crystal with $\theta = 60°$, which is mainly attributed to the excitation of Tamm plasmons. In addition, the magnetic field amplitude weakens when it is away from the metal, which further demonstrates that the excitation of the Tamm plasmons at the junction of the metal and magnetophotonic crystal. Correspondingly, the enhancement of magnetic field amplitude can achieve a high absorption at the wavelength of 15.760 μm. When $\theta = -60°$, the barely enhanced magnetic field leads to a weak absorption of the structure. Therefore, the different magnetic field distributions in opposite directions lead to the nonreciprocal radiation [35]. Figure 3(d) and (e) show the magnetic field distribution of the magnetophotonic crystal containing the defect layer at the wavelength of 14.750μm. Compared with the magnetic field distribution of the structure without the defect layer, the magnetic field intensity does not decrease when it is away from the metal, but increase and present the stationary wave mode along the z direction when z is between 5.8μm and 14.6μm, which is attributed to the Fabry-Perot resonance occurring in the defect layer. In addition, the excitation of Tamm plasmons can also be seen at the interface between metal and photonic crystals. What's more, in order to better understand the role of the defect layer in the photonic crystal, the reflection spectra of different structures are calculated respectively, as shown in Figure 3(c) and (f). It can be clearly seen that the presence of the defect splits the photonic band gap into two narrower band gaps, thus leading to the dual-band nonreciprocal thermal radiation [29].

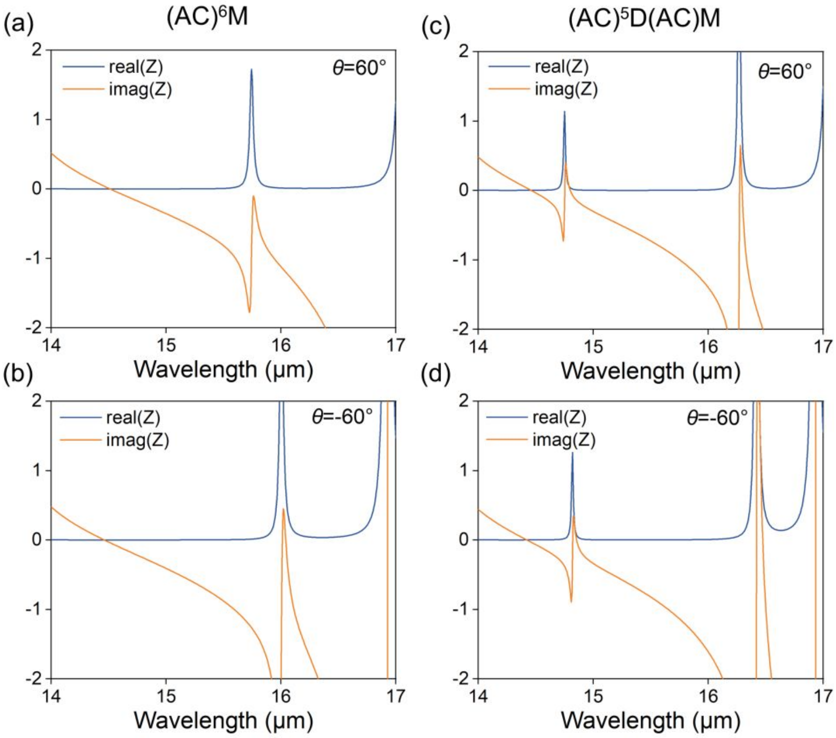

Figure 4. The effective impedance of the structure $(AC)^6M$ (a) at $\theta = 60°$ and (b) $\theta = -60°$ with $B = 3T$. The effective impedance of the structure $(AC)^5D(AC)M$ (c) at $\theta = 60°$ and (d) $\theta = -60°$ with $B = 3T$.

In order to deepen the understanding of the underlying physical mechanism, the effective impedance matching theory is adopted here for further explanation and specifically expressed as:

$$Z = \sqrt{\frac{(1+S_{11})^2 - S_{21}^2}{(1-S_{11})^2 - S_{21}^2}} \quad (8)$$

Here, S_{11} and S_{21} are the parameters related to scattering. In addition, because the bottom metal layer can block all transmissions, the parameter $|S_{21}|$ is equal to zero. Based on this, the effective impedances of the structures $(AC)^6M$ and $(AC)^5D(AC)M$ have been calculated respectively, as shown in Figure 4. First, when there is no defect layer, Z=0.969-0.101i with $\theta = 60°$ at the resonant wavelength of 15.760μm, which is matched to the free space impedance $Z_0=1$ so that there is a strong absorption. By contrast, Z=0.016-1.298i with $\theta = -60°$ at the resonant wavelength of 15.760μm, which is not matched so that there is a weak absorption. For the structure $(AC)^5D(AC)M$, the resonant wavelengths are 14.750 and 16.295μm with θ=60° and the corresponding effective impedances are 1.140-0.219i and 0.824+0.023i. However, with θ=-60°, the corresponding effective impedances are 0.022-0.376i and 0.091-3.126i, which is not matched to Z_0. Therefore, by calculating the effective impedance, the nonreciprocity can be better understood.

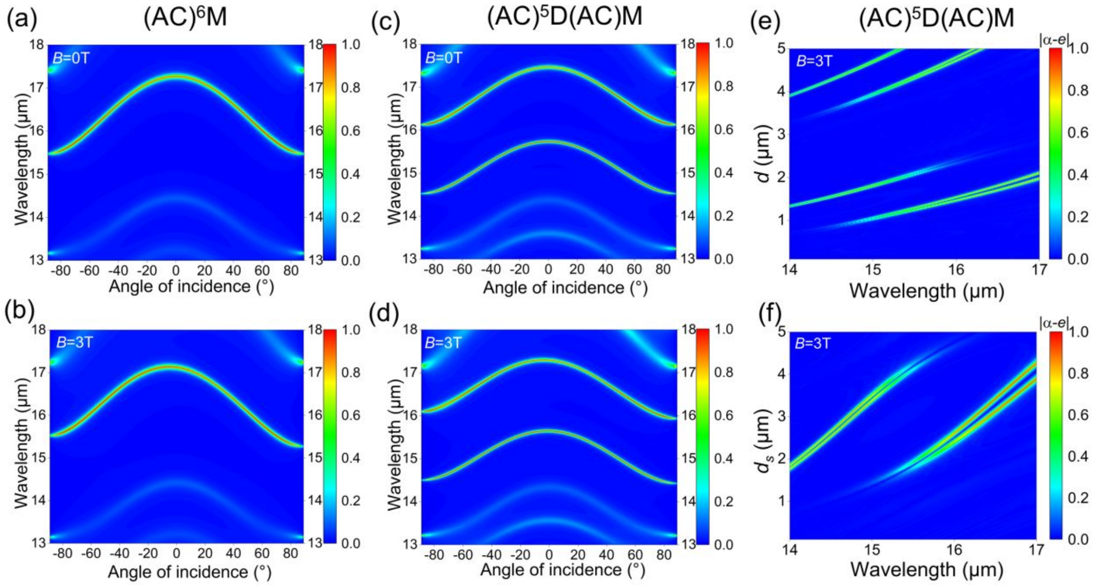

Figure 5. The absorptivity of the structure $(AC)^6M$ varies with the angle of incidence and wavelength: (a) B=0T, (b) B=3T. The absorptivity of the structure $(AC)^5D(AC)M$ varies with the angle of incidence and wavelength: (c) B=0T, (d) B=3T. (e) Difference between absorptivity and emissivity varies with the wavelength and the thickness of the InAs layer d. (f) Difference between absorptivity and emissivity varies with the wavelength and the thickness of the SiO_2 layer d_s.

The nonreciprocal thermal radiation is closely related to the incident angle. Here, the absorptivity as functions of the wavelength and incident angle with B=0T and 3T is shown in Figure 5(a-d). When there is no defect in the magnetophotonic crystal, the absorptivity is symmetric with respect to $\theta \to -\theta$ without the external excitation, as shown in Figure 5(a). As compared to the bands in Figure 5(a), the band at $\theta < 0°$ shifts upward and the band at $\theta > 0°$ shifts downward when B = 3T [Figure 5(b)]. The asymmetry absorptivity with respect to the angle of incidence shows the violation of Kirchhoff's law. Compared with the absorptivity spectra of the structure $(AC)^6M$, there are two obvious absorption bands in Figure 5(c) and (d). Similarly, when the B is applied in the structure $(AC)^5D(AC)M$, the bands will shift and the dual-band nonreciprocal thermal radiation will be achieved.

Figure 5(e) and (f) give the value of $|\alpha - e|$ varying with the thickness of the material and wavelength at θ= 60° with B = 3T. As shown in Figure 5(e), the thickness of InAs layer is changed from 0.1μm to 5μm, while keeping the thickness of SiO_2 unchanged. It can be seen that when d is in the range of 1.3μm-2.1μm and 4μm-5μm, dual-band nonreciprocal emitters can be obtained. Figure 5(f) shows the influence of d_s on the value of $|\alpha - e|$. The dual-band nonreciprocal radiation is realized when d_s is between 2μm and 4μm. Therefore, the dual-band nonreciprocal thermal emitter designed by this structure has a certain tolerance for size parameters.

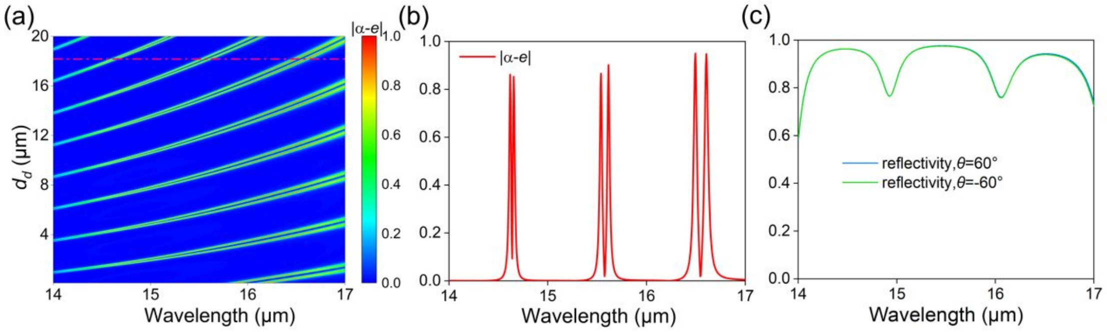

Figure 6. (a) Difference between absorptivity and emissivity varies with the wavelength and the thickness of the defect layer d_d. (b) the value of $|\alpha - e|$ when the thickness of defect layer is 18.2μm. (c) The reflectivity spectra for the structure $(AC)^5D(AC)$ at $\theta = 60°$ and -60° when the thickness of defect layer is 18.2μm.

Figure 6(a) discusses the influence of the defect layer thickness on the degree of nonreciprocity at $\theta = 60°$ with B = 3T. The value of $|\alpha - e|$ as the function of the wavelength and defect layer thickness is calculated and the thickness of d_d is changed from 0.1μm to 20μm. The multiple pairs of separated bands can be seen in the Figure 6(a), which represents the dual-band and even multi-band nonreciprocal radiation. Here, in order to show the effect of defect layer thickness on nonreciprocal thermal radiation more clearly, the difference between absorptivity and emissivity varying with the wavelength with d_d=18.2μm has been calculated which is the part marked with red dots in Figure 6(a), as shown in the Figure 6(b). It can be seen that the values of $|\alpha - e|$ at the wavelengths of 14.620μm, 15.615μm and 16.495μm can reach 0.862, 0.902 and 0.95, respectively. Such phenomenon shows that multi-band nonreciprocal thermal radiation also can be achieved by adjusting the thickness of the defect layer, which provides a new way for designing multi-band nonreciprocal emitters. In addition, the reflectivity spectra for the structure $(AC)^5D(AC)$ at $\theta = 60°$ and -60° when the thickness of defect layer is 18.2μm are calculated, as shown in Figure 6(c). Compared with the reflection spectra of the photonic crystal without the defect [Figure 3(c)], the complete photonic band gap is divided into three narrower photonic band gaps, corresponding to the tri-band nonreciprocal thermal radiation. Therefore, with the increase of defect layer thickness, more defect modes in the photonic band gap may lead to the realization of multi-band nonreciprocal thermal radiation [29].

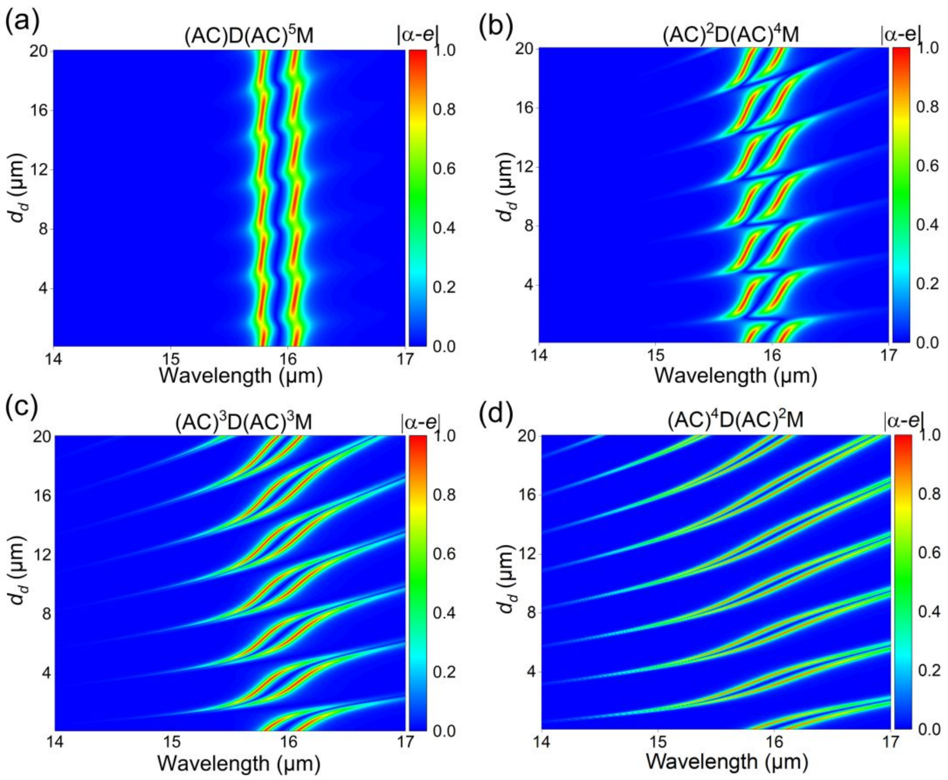

Figure 7. Difference between absorptivity and emissivity varies with the wavelength and the thickness of the defect layer d_d for different structures: (a) (AC)D(AC)^{5}M, (b) (AC)^{2}D(AC)^{4}M, (c) (AC)^{3}D(AC)^{3}M, (d) (AC)^{4}D(AC)^{2}M.

In order to verify whether the influence of the location of the defect on the multi-band nonreciprocal thermal radiation is accidental, the nonreciprocities under different defect locations are discussed, as shown in Figure 7. For structures (AC)D(AC)^{5}M and (AC)^{2}D(AC)^{4}M, as shown in Figure 7(a) and (b), there are two obvious nonreciprocal bands near 16μm, which represents single-band nonreciprocal thermal radiation. In this case, even if there is a defect in the photonic crystal, it cannot form dual-band or even multi-band nonreciprocal thermal radiation well, mainly because the two ends of the defect layer are not highly reflective interfaces, which cannot form FP resonance. As the location of the defect layer gradually approaches the metal layer, as shown in Figure 7(c) and (d), it can be obviously seen that multiple pairs of separation bands appear with the increase of the thickness of the defect layer, representing dual-band and multi-band nonreciprocal thermal radiation. Therefore, by studying the effect of the location of the defect layer on the nonreciprocity, on the one hand, it shows that adding the defect layer to the photonic crystal can indeed achieve the regulation of multi-band nonreciprocal thermal radiation. On the other hand, it is also verified that whether FP resonance can occur in the defect layer is an important prerequisite for the realization of multi-band nonreciprocal thermal radiation.

4. Conclusion

In summary, the emitter composed by magnetophotonic crystal with defect layer and a metal layer can realize the dual-band nonreciprocal thermal radiation at $\theta = 60°$ with B = 3T. The realization of dual-band nonreciprocal radiation is attributed to the FP resonance occurring in the defect layer and the excitation of Tamm plasmon, which can be demonstrated by calculating the magnetic field distribution. What's more, the defect layer thickness plays an important role in the number of nonreciprocal bands. When the thickness of the defect increases to 18.2μm, tri-band nonreciprocal radiation is realized due to the enhanced number of defect modes in photonic band gap. Finally, the location of the defect layer also has a great influence on the nonreciprocity, mainly because the location of the defect layer plays a crucial role in the formation of FP resonance. We believed that this work can provide new ways to design multi-band or even broadband nonreciprocal thermal emitters of practical interests.

Acknowledgments

The authors would like to acknowledge the financial support by National Natural Science Foundation of China (52211540005, 52076087), and the Open Project Program of Wuhan National Laboratory for Optoelectronics (2021WNLOKF004), Wuhan Knowledge Innovation Shuguang Program, and Science and Technology Program of Hubei Province (2021BLB176).

References

[1] Dalapati GK, Kushwaha AK, Sharma M, et al. Transparent heat regulating (thr) materials and coatings for energy saving window applications: Impact of materials design, micro-structural, and interface quality on the thr performance. Prog Mater Sci, 2018, 95: 42-131

[2] Fan S. Thermal photonics and energy applications. Joule, 2017, 1(2): 264-273

[3] Seyf HR, Henrya A. Thermophotovoltaics: A potential pathway to high efficiency concentrated solar power. Energy Environ Sci, 2016, 9(8): 2654-2665

[4] Liu P, Ren T, Ge Y, et al. Performance analyses of a novel finned parabolic trough receiver with inner tube for solar cascade heat collection. Sci China Technol Sci, 2023, 66(5): 1417-1434

[5] Baranov DG, Xiao YZ, Nechepurenko IA, et al. Nanophotonic engineering of far-field thermal emitters. Nat Mater, 2019, 18(9): 920-930

[6] Li W, Fan SH. Nanophotonic control of thermal radiation for energy applications [invited]. Opt Express, 2018, 26(12): 15995-16021

[7] Kirchhoff G. Ueber das verhältniss zwischen dem emissionsvermögen und dem absorptionsvermögen der körper für wärme und licht. Annalen der Physik und Chemie, 1860, 185(2): 275-301

[8] Zhang ZM, Wu X, Fu C. Validity of kirchhoff's law for semitransparent films made of anisotropic materials. J Quant Spectrosc Ra, 2020, 245: 106904

[9] Rephaeli E, Fan SH. Absorber and emitter for solar thermophotovoltaic systems to achieve efficiency exceeding the shockley-queisser limit. Opt Express, 2009, 17(17): 15145-15159

[10] Snyder WC, Wan ZM, Li XW. Thermodynamic constraints on reflectance reciprocity and kirchhoff's law. Appl Opt, 1998, 37(16): 3464-3470

[11] Buddhiraju S, Santhanam P, Fan SH. Thermodynamic limits of energy harvesting from outgoing thermal radiation. PNAS, 2018, 115(16): E3609-E3615

[12] Zang H, Li H, Liang T, et al. Goldilocks focal zone in femtosecond laser ignition of lean fuels. Sci China Technol Sci, 2022, 65(7): 1537-1544

[13] Han SE. Theory of thermal emission from periodic structures. Physical Review B, 2009, 80(15): 155108

[14] Zhu L, Fan S. Near-complete violation of detailed balance in thermal radiation. Phys Rev B, 2014, 90(22): 220301

[15] Zhao B, Guo C, Garcia CAC, et al. Axion-field-enabled nonreciprocal thermal radiation in weyl semimetals. Nano Lett, 2020, 20(3): 1923-1927

[16] Liu MQ, Zhao CY. Near-infrared nonreciprocal thermal emitters induced by asymmetric embedded eigenstates. Int J Heat Mass Tran, 2022, 186: 122435

[17] Zhao B, Shi Y, Wang J, et al. Near-complete violation of kirchhoff's law of thermal radiation with a 0.3 t magnetic field. Opt Lett, 2019, 44(17): 4203-4206

[18] Wu F, Wu JJ, Guo ZW, et al. Giant enhancement of the goos-hanchen shift assisted by quasibound states in the continuum. Phys Rev Appl, 2019, 12(1): 014028

[19] Wu J, Wu F, Zhao T, et al. Dual-band nonreciprocal thermal radiation by coupling optical tamm states in magnetophotonic multilayers. Int J Therm Sci, 2022, 175: 107457

[20] Wu J, Wu F, Wu X. Strong dual-band nonreciprocal radiation based on a four-part periodic metal grating. Opt Mater, 2021, 120: 111476

[21] Wu X, Liu R, Yu H, et al. Strong nonreciprocal radiation in magnetophotonic crystals. J Quant Spectrosc Ra, 2021, 272: 107794

[22] Wu J, Li H, Fu C, et al. High quality factor nonreciprocal thermal radiation in a weyl semimetal film via the strong coupling between tamm plasmon and defect mode. Int J Therm Sci, 2023, 184: 107902

[23] Luo M, Xu Y, Xiao Y, et al. Strong nonreciprocal thermal radiation by optical tamm states in weyl semimetallic photonic multilayers. Int J Therm Sci, 2023, 183: 107851

[24] Tsurimaki Y, Qian X, Pajovic S, et al. Large nonreciprocal absorption and emission of radiation in type-i weyl semimetals with time reversal symmetry breaking. Phys Rev B, 2020, 101(16): 165426

[25] Ning RX, Jiao Z, Bao J. Tunable multi-band absorption in metasurface of graphene ribbons based on composite structure. European Physical Journal-Applied Physics, 2017, 79(1): 10201

[26] Liu YJ, Xie X, Xie L, et al. Dual-band absorption characteristics of one-dimensional photonic crystal with graphene-based defect. Optik, 2016, 127(9): 3945-3948

[27] Wu J, Qing YM. Strong nonreciprocal radiation with topological photonic crystal heterostructure. Appl Phys Lett, 2022, 121(11): 112201

[28] Zhang Z, Zhu L. Broadband nonreciprocal thermal emission. Phys Rev Appl, 2023, 19(1): 014013

[29] Wu J, Qing YM. A multi-band nonreciprocal thermal emitter involving a weyl semimetal with a thue-morse multilayer. Phys Chem Chem Phys, 2023, 25(16): 11477-11483

[30] Chen Z, Yu S, Hu B, et al. Multi-band and wide-angle nonreciprocal thermal radiation. Int J Heat Mass Transfer, 2023, 209: 124149

[31] Fang YT, Zheng J. Optical isolator based on nonreciprocal coupling of two tamm plasmon polaritons. Radiat Eff Defects Solids, 2014, 169(12): 1010-1018

[32] Qi L, Yang Z, Fu T. Defect modes in one-dimensional magnetized plasma photonic crystals with a dielectric defect layer. Phys Plasma, 2012, 19(1): 012509

[33] Wu CJ, Wang ZH. Properties of defect modes in one-dimensional photonic crystals. Progress in Electromagnetics Research-Pier, 2010, 103: 169-184

[34] King TC, Wu CJ. Properties of defect modes in one-dimensional symmetric defective photonic crystals. Physica E-Low-Dimensional Systems & Nanostructures, 2015, 69: 39-46

[35] Wu J, Wang ZM, Wu BY, et al. The giant enhancement of nonreciprocal radiation in thue-morse aperiodic structures. Optics and Laser Technology, 2022, 152: 108138

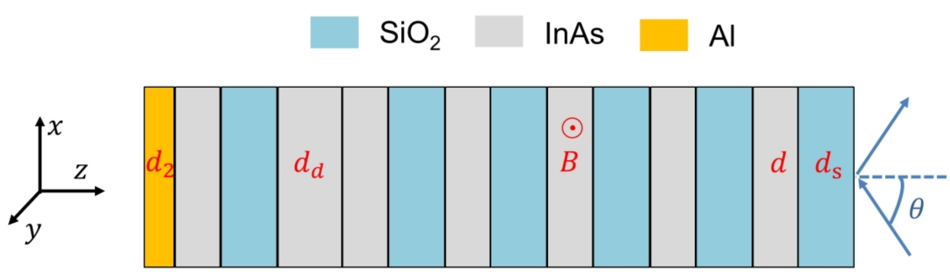

Figure 1. Schematic of magnetophotonic crystal multilayer structure containing the defect layer.

209x190mm (300 x 300 DPI)

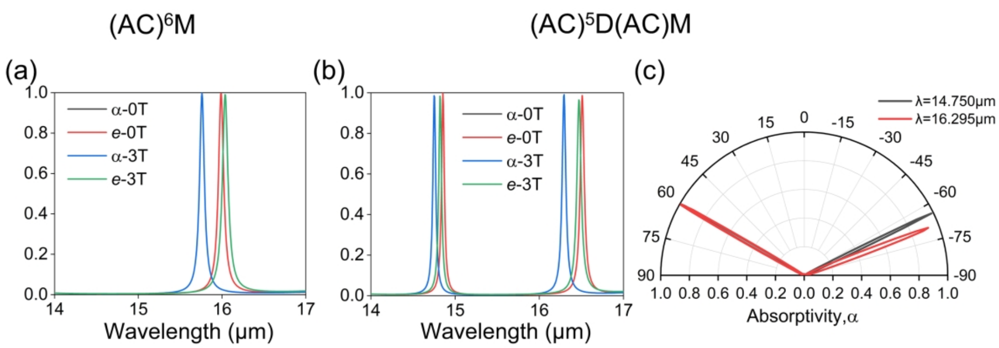

Figure 2. Absorptivity (ɑ) and emissivity (e) spectra at θ=60° with B = 0T and B = 3T: (a) the structure without the defect layer ((AC)6M), (b) the structure with the defect layer ((AC)5D(AC)M). (c) Angular distribution diagram of absorptivity at the resonant wavelengths with B = 3T for the structure (AC)5D(AC)M.

209x190mm (300 x 300 DPI)

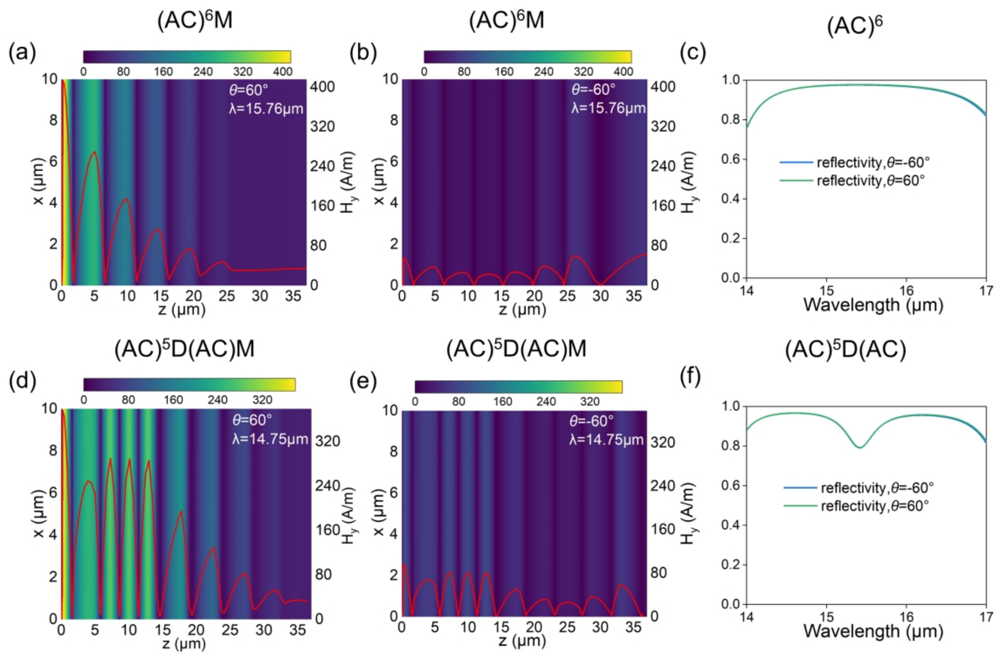

Figure 3. Magnetic field distribution (|Hy|) of the structure (AC)6M along the z direction at the wavelength of 15.760μm (a) at θ= 60° and (b) θ= -60° with B = 3T. (c) The reflectivity spectra for the structure (AC)6 at θ=60° and -60°. Magnetic field distribution (|Hy|) of the structure (AC)5D(AC)M along the z direction at the wavelength of 14.750μm (d) at θ= 60° and (e) θ= -60° with B = 3T. (f) The reflectivity spectra for the structure (AC)5D(AC) at θ= 60° and -60°.

209x190mm (300 x 300 DPI)

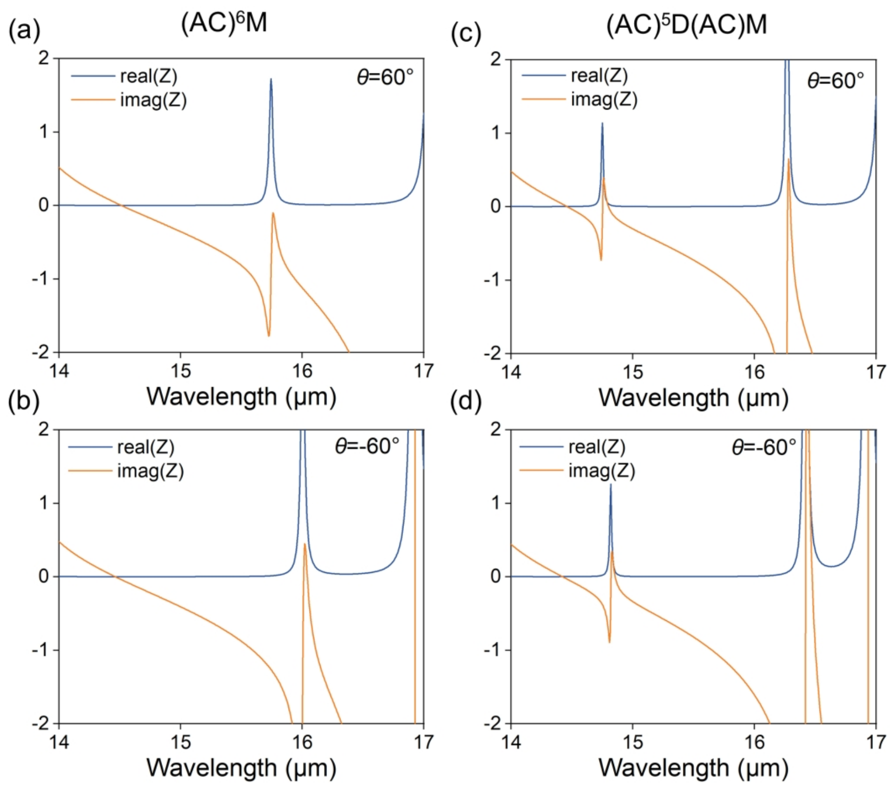

Figure 4. The effective impedance of the structure (AC)6M (a) at θ= 60° and (b) θ= -60° with B = 3T. The effective impedance of the structure (AC)5D(AC)M (c) at θ= 60° and (d) θ= -60° with B = 3T.

209x190mm (300 x 300 DPI)

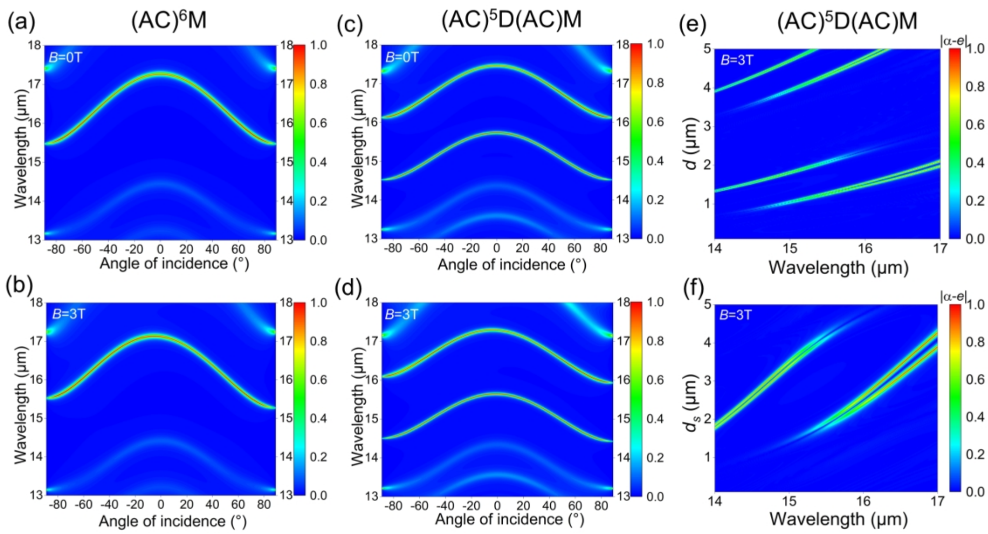

Figure 5. The absorptivity of the structure (AC)6M varies with the angle of incidence and wavelength: (a) B=0T, (b) B=3T. The absorptivity of the structure (AC)5D(AC)M varies with the angle of incidence and wavelength: (c) B=0T, (d) B=3T. (e) Difference between absorptivity and emissivity varies with the wavelength and the thickness of the InAs layer d. (f) Difference between absorptivity and emissivity varies with the wavelength and the thickness of the SiO2 layer ds.

209x190mm (300 x 300 DPI)

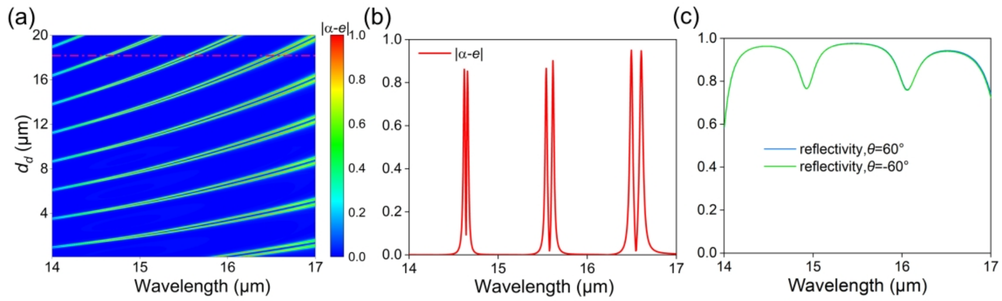

Figure 6. (a) Difference between absorptivity and emissivity varies with the wavelength and the thickness of the defect layer dd. (b) the value of |ɑ-e| when the thickness of defect layer is 18.2μm. (c) The reflectivity spectra for the structure (AC)5D(AC) at θ= 60° and -60° when the thickness of defect layer is 18.2μm.

209x190mm (300 x 300 DPI)

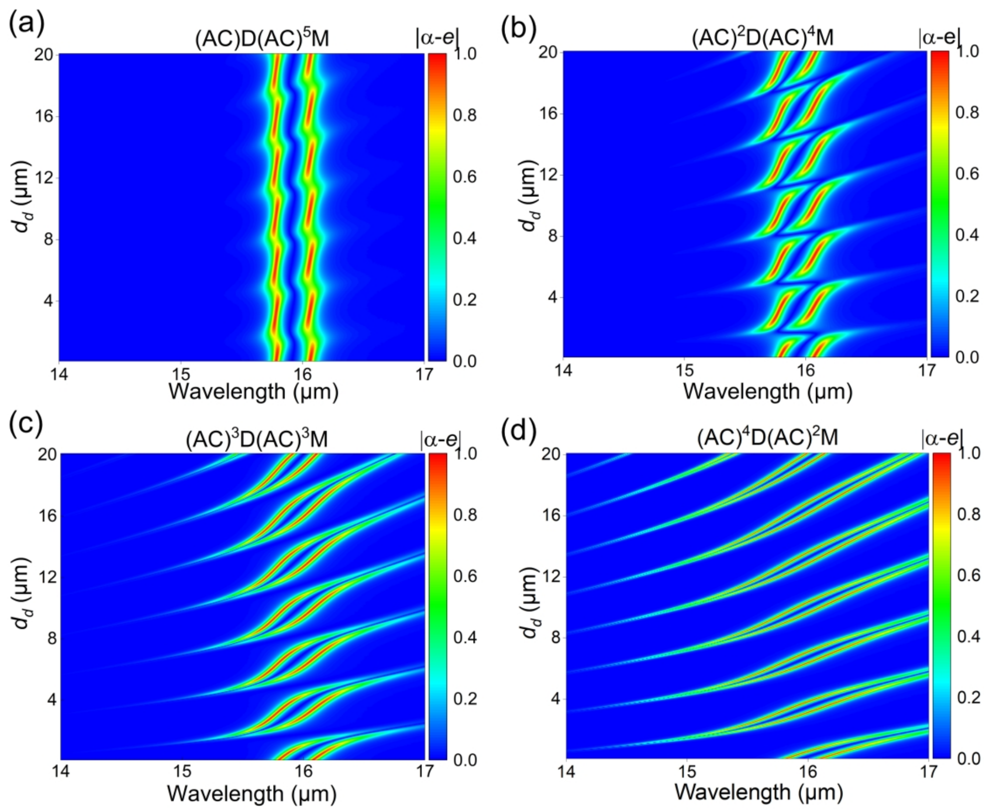

Figure 7. Difference between absorptivity and emissivity varies with the wavelength and the thickness of the defect layer dd for different structures: (a) (AC)D(AC)5M, (b) (AC)2D(AC)4M, (c) (AC)3D(AC)3M, (d) (AC)4D(AC)2M.

209x190mm (300 x 300 DPI)